# EXPLORING NICKEL NANOPARTICLE SYNTHESIS THROUGH LASER ABLATION IN LIQUID

Alexandru-Mihai IAMANDI[1,2]*, Liviu – Daniel GHICULESCU[3], Alexandru-DAN[5], Anca CRIVEANU[6], Ioan-GHITIU[7], Nicu Doinel SCĂRIȘOREANU[4]

1 Universitatea Națională de Știință și Tehnologie POLITEHNICA București, alexandru.iamandi@gmail.com
2 Institutul Național pentru Fizica Laserilor, Plasmei și Radiației alexandru.iamandi@gmail.com
3 Universitatea Națională de Știință și Tehnologie POLITEHNICA București, daniel.ghiculescu@gmail.com
4 Institutul Național pentru Fizica Laserilor, Plasmei și Radiației, nicu.scarisoreanu@inflpr.ro
5 Institutul Național pentru Fizica Laserilor, Plasmei și Radiației, alexandru.dan@inflpr.ro
6 Institutul Național pentru Fizica Laserilor, Plasmei și Radiației, anca.criveanu@inflpr.ro
7 Institutul Național pentru Fizica Laserilor, Plasmei și Radiației, ioan.ghitiu@inflpr.ro

ABSTRACT: Metallic nanoparticles are of considerable importance in various industrial domains due to their unique properties, including a high surface area-to-volume ratio and exceptional catalytic activity. These nanoparticles are widely utilized in fields such as catalysis, electronics, and biomedicine, where they significantly enhance efficiency and performance. This study reports the synthesis of nickel nanoparticles via laser ablation in liquid, employing a 99% pure nickel target, and their characterization using several analytical techniques, including Dynamic Light Scattering (DLS), Atomic Force Microscopy (AFM), Scanning Electron Microscopy (SEM), Energy-Dispersive X-ray Spectroscopy (EDX) and TEM (Transmission electron microscopy). The resulting nanoparticles exhibited sizes ranging from 7 to 40 nm, possessing both anionic and cationic characteristics, along with a narrow size distribution and excellent stability. For the experiments, wavelengths of 1064, 532, and 355 nm were employed, with a pulse frequency of 10 Hz and an ablation duration of 20 minutes, corresponding to a total of 12,000 pulses. Ultrapure water and ultrapure water with various concentrations of NaCl were used as liquid suspensions.

KEYWORDS: Pulsed laser ablation, nanoparticle, nanostructures, target, SEM, TEM

## 1. INTRODUCTION

In recent years, magnetic nanoparticles have become integral components in numerous technological breakthroughs, showcasing vast potential for diverse applications. Nickel (Ni) nanoparticles have particularly garnered attention due to their unique magnetic properties. The amalgamation of these nanostructures presents an intriguing opportunity to push the boundaries of Ni nanoparticles synthesized via laser ablation exhibit unique characteristics that make them highly desirable for various applications. Their size-dependent magnetic behaviour, coupled with high saturation magnetization, renders them invaluable in magnetic recording, biomedical applications, and catalysis. Additionally, the controlled synthesis process enables the production of uniform nanoparticles with tailored properties, ensuring consistency and reproducibility in applications requiring precise magnetic properties [13,14].

Nanoparticles can be synthesized through a variety of methods, typically classified into two main approaches: top-down and bottom-up. Each method has its own advantages and is chosen based on the desired nanoparticle size, shape, composition, and application.[1]

**Top-down methods**: These methods involve breaking down materials from solid targets into nanoparticles. They are generally used when precise control over shape is less critical, but a disadvantage is that they tend to be energy-intensive.

- Ball Milling

Involves mechanical grinding of bulk materials into nanoscale particles. [2]

Typically used for producing metal or ceramic nanoparticles.

Advantages: Simple, scalable.

Disadvantages: Poor control over particle size and shape.

- Laser Ablation

A high-energy laser beam is directed at a bulk material, causing its vaporization and condensation into nanoparticles. [3]

Suitable for producing metal, semiconductor, and oxide nanoparticles.

Advantages: High purity and uniform size distribution.

Disadvantages: Expensive equipment, low throughput.

- Lithography

Uses focused beams of electrons or light to carve out nanostructures from a solid material. [4]

Commonly used in the semiconductor industry.

Advantages: Very precise size and shape control.

Disadvantages: Limited to small-scale production.

- Etching

Chemical or physical removal of material from the surface, leaving behind nanoparticle structures. [5]

Often used for semiconductor nanomaterials.

Advantages: High precision.

Disadvantages: Complex setup and control.

**Bottom-Up Methods:** These methods involve building nanoparticles from atoms or molecules. They generally offer better control over particle size, shape, and composition.

- **Sol-Gel Process**

Involves the transition from a colloidal solution (sol) to a solid (gel), followed by controlled heating to form nanoparticles. [6]

Commonly used for oxide materials like silica or titanium dioxide.

Advantages: Low-cost, uniform size distribution.

Disadvantages: Time-consuming, requires precise control over reaction conditions.

- **Chemical Vapor Deposition (CVD)**

A gaseous reactant is introduced into a chamber where it undergoes a chemical reaction and deposits onto a substrate, forming nanoparticles. [7]

Widely used for producing carbon nanotubes and semiconductor nanoparticles.

Advantages: High purity and uniformity.

Disadvantages: High temperatures, expensive.

- **Precipitation Method**

Involves the mixing of two solutions to cause the precipitation of nanoparticles from a supersaturated solution. [8]

Frequently used for metal and metal oxide nanoparticles.

Advantages: Simple and scalable.

Disadvantages: Requires precise control over concentration and temperature to avoid agglomeration.

- **Hydrothermal and Solvothermal Synthesis**

Nanoparticles are synthesized in high-temperature and high-pressure water or solvent solutions. [9]

Used for producing metal oxides, sulfides, and other inorganic nanoparticles.

Advantages: Good control over particle size and crystallinity.

Disadvantages: Requires specialized equipment.

- **Microemulsion Method**

Nanoparticles are synthesized within tiny droplets of water dispersed in oil, stabilized by surfactants. [10]

Often used for producing metal nanoparticles.

Advantages: Excellent control over size and shape.

Disadvantages: Complex separation processes required after synthesis.

- **Biological Synthesis (Green Synthesis)**

Involves the use of biological organisms like bacteria, fungi, plants, or enzymes to produce nanoparticles. [11]

Mainly used for metal nanoparticles like silver, gold, and platinum.

Advantages: Eco-friendly, low toxicity.

Disadvantages: Low yield and slower reaction times.

This paper presents the results obtained after the laser ablation process in liquid, using a solid target of Nickel 99% purity.

In this article, we aim to elucidate the synthesis process of nickel nanoparticles, followed by their characterization employing various methodologies including Dynamic Light Scattering (DLS), Scanning Electron Microscopy (SEM), Energy Dispersive X-ray Spectroscopy (EDX), and Atomic Force Microscopy (AFM). Understanding the synthesis of Ni nanoparticles via laser ablation not only expands our knowledge of nanomaterial fabrication but also opens doors to innovative technologies with enhanced performance and functionality. This review aims to provide insights into the synthesis process and applications of laser-ablated Ni nanoparticles, contributing to the advancement of nanoscience and technology.

## 2. EXPERIMENTAL SETUP

The laser ablation process was conducted utilizing a Pulsed Quantel QSMART 850 laser operating at 1064 nm, and employing Q-switching at delays of 150, 100, and 50 microseconds, and a Nd-YAG Continuum laser working at 1064, 532 and 355nm wavelengths. The 99.999 purity nickel target was positioned at the base of the reaction chamber, situated on a holder located 2.5 cm from the base of the target. The laser beam was directed onto the target surface using mirrors arranged in the optical path, with an energy range of approximately 350-660 mJ for the laser ablation process. The reaction chamber was mounted on a translation stage to facilitate laser beam scanning along the X-axis, while adjustable mounts were utilized to control scanning along the Y-axis. The nickel target was immersed in ultrapure water (UPW) or ultrapure water containing 5 and 10 mlM of NaCl.

In the design of the optical setup (figure 1), the position of the laser and the entrance aperture of the laser beam into the ablation chamber were considered. With these aspects in mind, the laser beam must be strategically directed to penetrate through the top of the ablation chamber.

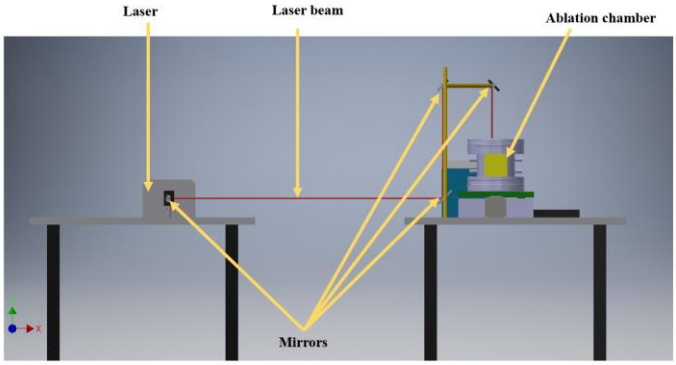


**Figure 1.** Lateral view of setup

Considering this particularity, it was found necessary to use four mirrors to direct the beam (see figure 2). The final mirror will be used to adjust the beam on the Y-axis of the target, controlled via a laptop (see figure 2.1).

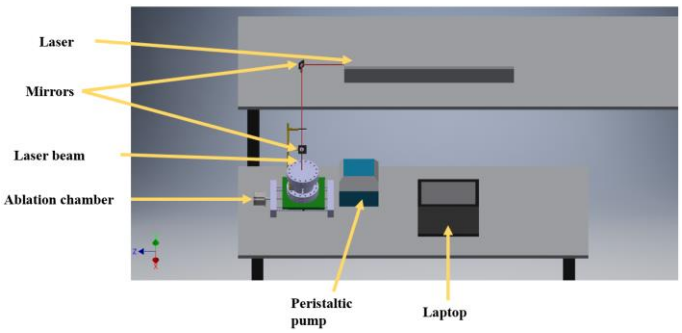


**Figure 2.** Top view of the designed setup

Figure 3 shows the experimental setup used in the liquid laser ablation process. The picture shows the ablation camera fixed on the translation table to facilitate the direction of the laser beam in the X-axis. To control the direction in the Y-axis, a Kinesis K-Cube Brushed DC Servo Motor Controller manufactured by Thorlabs was used. This single channel controller has been designed to allow both manual and automatic control of DC servo motors. Its capability includes driving a wide range of low power (up to 15 V/2.5 W) brushed DC motors equipped with encoder feedback

The mirrors used for guiding the laser beam and for Y-axis scanning are manufactured by Thorlabs and are designed to handle the fundamental, second, third and fourth harmonic wavelengths of the lasers Nd: YAG. They are coated with dielectric layers that provide effective reflectance for S and P polarized light while exhibiting outstanding resistance to damage. Each coating layer is adapted to operate at angles of incidence (AOI - the angle at which a collimated light beam strikes the first surface of the filter, measured relative to the surface normal) between 0° and 45°, which allows them to be used in a variety of optical arrangements.

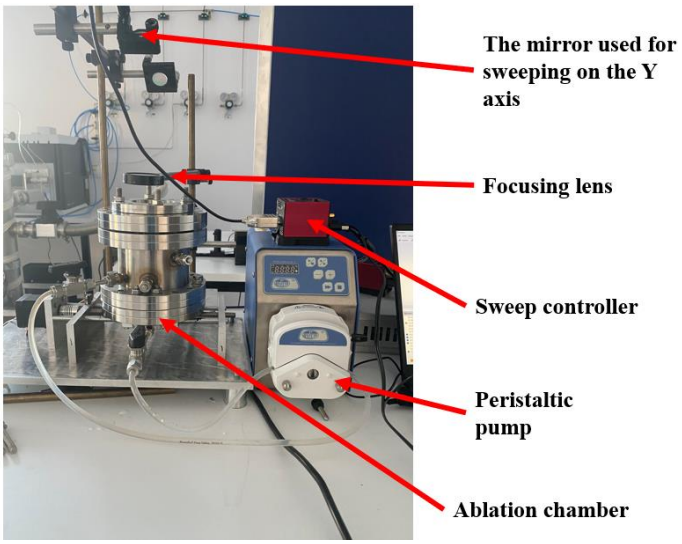


**Figure 3.** The experimental set

To implement the X-axis targeting system of the liquid ablation chamber, the electrical connections were configured according to the program developed in the previous subchapter and as specified in the TB6600 driver data sheet. The complete hardware configuration can be seen in figure 4.

Pins 5, 2 and 8 of the Arduino development board were connected to the STEP, DIRECTION and ENABLE pins of the TB6600 driver. The stepper motor connections were made according to the specifications in its datasheet, respecting the corresponding connections of each coil on the

TB6600 driver. Afterwards, the connections to the voltage source for the driver and the Arduino Nano development board were also made. During the experiments, the driver settings used were as follows: 2/8 micro stepping, 400 micro stepping/revolution (off-on-on), 2.8A (off-off-off).

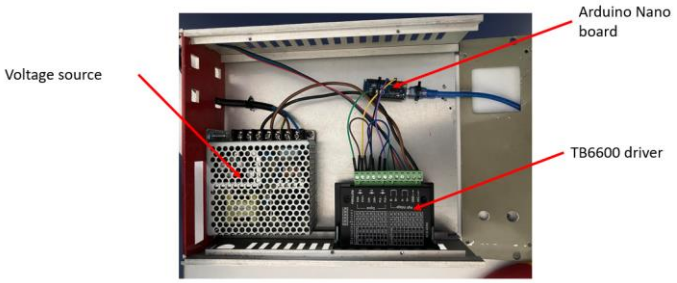


**Figure 4.** Hardware configuration

## 3. RESULTS AND DISCUSSION

Several experiments were conducted using the Quantel laser at a 50 µs Q-switch and a frequency of 10Hz and experiments with Continuum laser for 1064, 532 and 355nm wavelengths and a frequency of 10 Hz. Within the ablation chamber, volumes ranging from 300 to 400 ml of ultrapure water and ultrapure water solution with 5/10 ml NaCl were introduced. The chamber fluid was then recycled using a peristaltic pump at a flow rate of 50 ml/min.

The nanoparticles obtained through the liquid-phase laser ablation process underwent characterization using various analytical techniques, including Dynamic Light Scattering (DLS), Atomic Force Microscopy (AFM), Scanning Electron Microscopy (SEM), and Energy Dispersive X-ray Spectroscopy (EDX). Characterization yielded a range of data, including:

- Nanoparticle size
- Dispersion of nanoparticles in liquid suspension
- Nanoparticle type
- Zeta potential

This graph from below (figure 5) demonstrates a nanoparticle sample with a well-defined, uniform particle size around 100 nm (the distribution seems to center around **100 nm**, indicating that most particles are in the range of approximately 100 nanometers in size. On X-axis). DLS is commonly used in nanoparticle research for determining the hydrodynamic diameter of particles dispersed in a solution, and the results here suggest that the synthesis process has yielded particles with a relatively consistent size.

On Y-axis (Frequency %) the peak of the distribution occurs around 100 nm, showing that the majority of particles are close to this diameter. The frequency distribution is relatively narrow, implying that the sample has a fairly uniform size distribution, with most particles concentrated around the 100 nm size range.

The right Y-axis (Undersize %) this axis provides the cumulative percentage of particles that are smaller than a particular diameter. As the diameter increases, the percentage approaches 100%, indicating that nearly all particles are within a small range.

On average, the obtained samples have a polydispersity index of less than 0.7, indicating a narrow size distribution. From the obtained data for the zeta potential of the analyzed samples (for example, 37.9, 42.2, 24.5, 25.3 mV), nanoparticles with cationic character (zeta potentials exceeding +30 mV are considered strongly cationic) as well as nanoparticles with anionic character (which decrease below -30 mV are classified as strongly anionic) were obtained. The images (fig 5) below show a series of DLS data obtained for the characterization of nanoparticles.

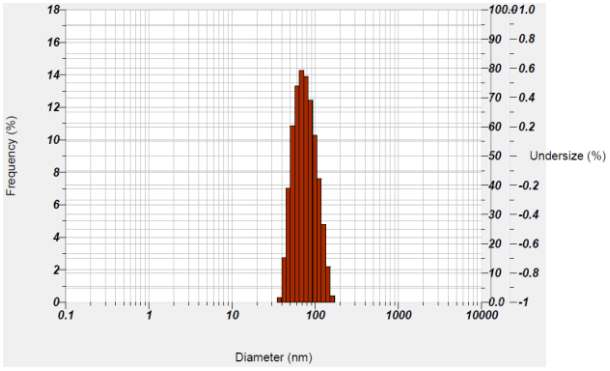


**Figure 5.** DLS analysis

In order to identify the constituent elements of the nanoparticles, an EDX (Energy-Dispersive X-ray Spectroscopy) analysis was performed (see figure 6) for the sample. As a result of this analysis, the following elements were identified: silicon (Si), nickel (Ni), oxygen (O), Al (Aluminum), Fe (Iron) and carbon (C).

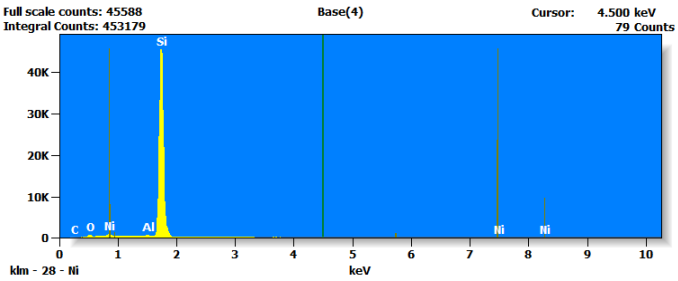


**Figure 6.** EDX analysis

This spectrum represents a sample composed mainly of silicon (Si) which is represented by the plate on which the nanoparticle suspension was deposited to

be able to analyze nickel (Ni) with traces of carbon (C), oxygen (O) and aluminum (Al). The intensities of these elements indicate their relative abundance within the sample, with silicon and nickel being the most prominent based on peak height.

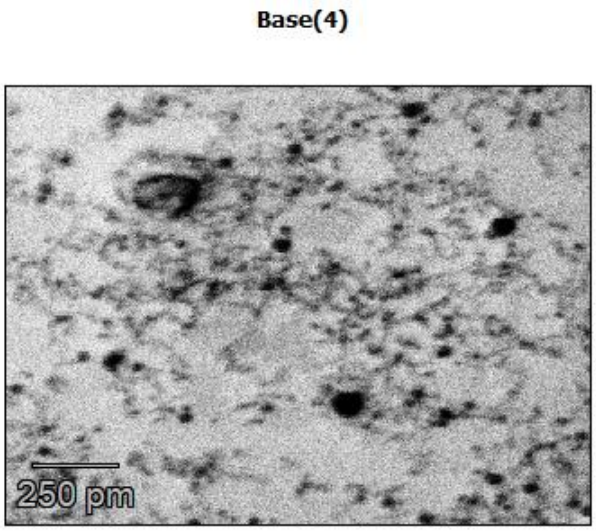


**Figure 7.a.** EDX analyzed area

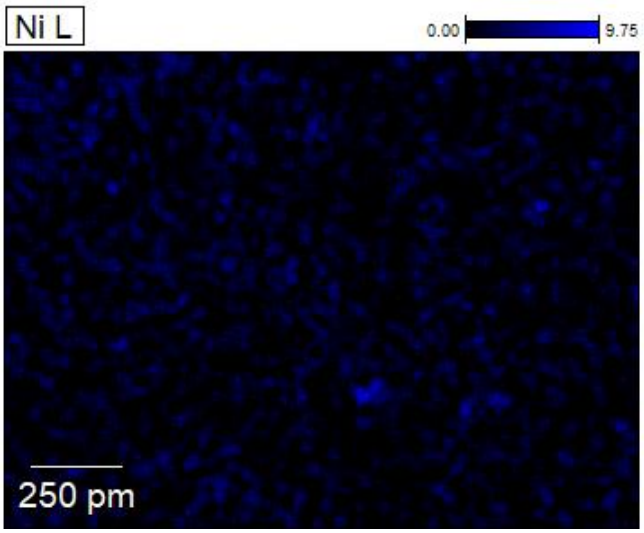


**Figure 7.b.** EDX nickel mapping

From the images above, a) the analyzed area and b) it shows that Nickel is distributed in small clusters or is relatively dispersed across the field of view. The concentration appears low overall, as indicated by the mostly dark color, with brighter spots suggesting higher concentrations of Nickel in certain areas. This mapping helps to visualize how Nickel is distributed within the sample.

AFM (Atomic Force Microscopy) was performed on the on probes, to characterize (see figure 8,9) the nanoparticles that we obtain from laser ablation in liquid. The main image shows the topography of a nanoparticle sample. The colour map (from dark orange to bright yellow/white) represents the height variations on the surface, where brighter areas are higher and correspond to nanoparticles, while darker areas represent the spaces between them. The scale bar on the left indicates height, in nanometres (nm), showing the vertical dimension of the nanoparticles on the substrate. The nanoparticles appear to be relatively uniform in size and densely packed across the surface.

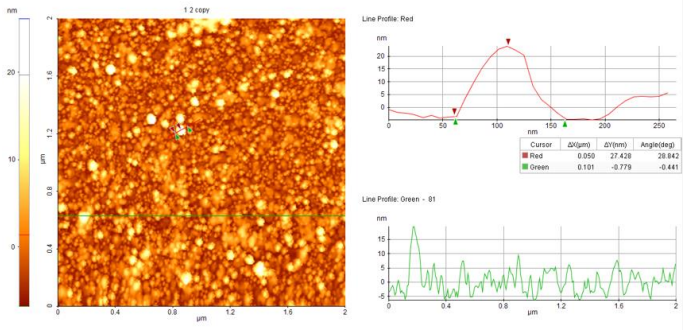

**Figure 8.** AFM characterization probe, 1064nm, Qswitch 50, 400ml UPW

The top-right graph shows a line profile across the surface, highlighting the height variations of individual nanoparticles. Peaks in this graph correspond to individual nanoparticles or clusters, while valleys are the spaces between them.

The bottom-right graph shows a similar cross-sectional profile along a different axis or area of the surface. It also emphasizes the size distribution and spacing between nanoparticles.

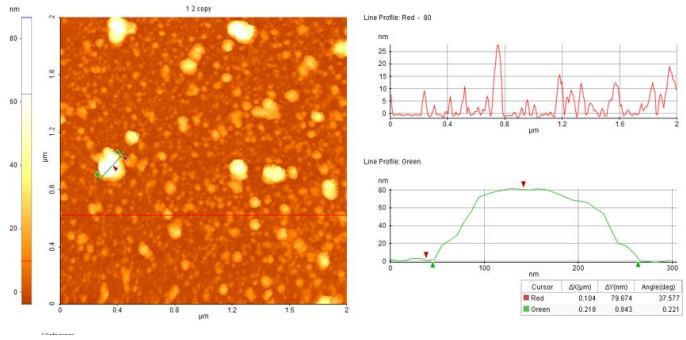

**Figure 9.** AFM characterization probe, 1064nm, Qswitch 50, 400ml UPW

The histogram provides a distribution of nanoparticle heights. The X-axis represents the height (in nm), and the Y-axis shows the frequency of those heights. A narrow peak in the histogram would suggest uniform nanoparticle size, while a broader peak would indicate a wider size distribution. The particles likely have a range of heights, with most heights clustered around the peak of the histogram. In the second AFM image you can see a uniform distribution of small nanoparticles (respectively 25nm) but also nanoparticles with larger sizes, respectively 90 nm.

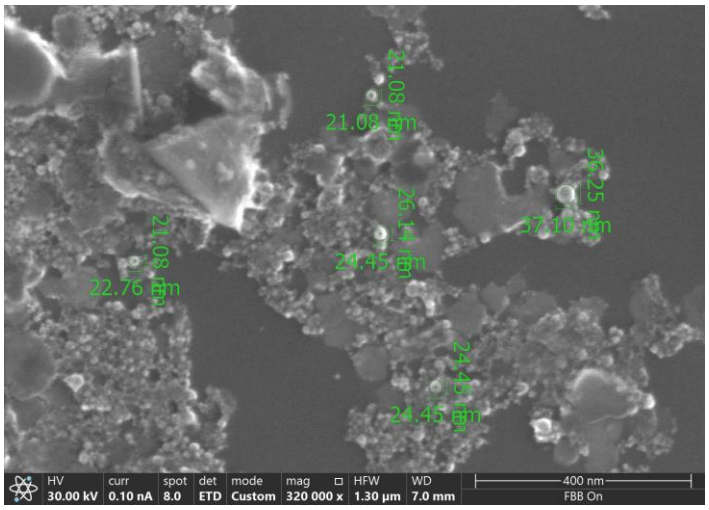


**Figure 10.** SEM characterization probe, 1064nm, Qswitch 100, 400ml UPW+4mlM NaCl

In image above (figure 10) scanning electron microscopy (SEM) image of the nanoparticles obtained. These images show nanoparticles characterized by an almost spherical shape, with sizes between 7 and 40 nm, together with aggregates of nanoparticles formed in the associated liquid suspension. A magnification of 320,000x and a HFW (Horizontal Field Width) of 1.30µm were used. For the sample presented above, a wavelength of 1064nm was used, the suspension used being ultrapure water with 4mlM NaCl, Qswitch 100 and a peristaltic pump flow rate of 50ml/min

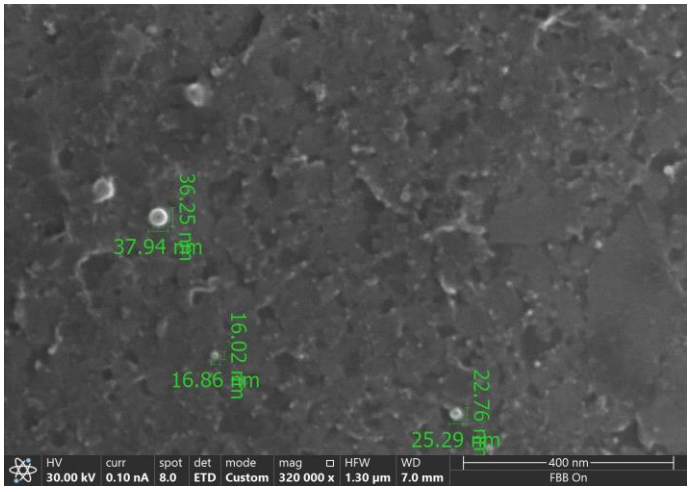


**Figure 11.** SEM characterization probe, 532nm, 300ml UPW

For the sample presented above (figure 11), a wavelength of 532nm, 10Hz frequency was used, the suspension used being ultrapure water and a peristaltic pump flow rate of 50ml/min.

For the sample presented below, a wavelength of 355nm was used, the suspension used being ultrapure water with 4mlM NaCl, Qswitch 100 and a flow rate of the peristaltic pump of 50 ml/min. As can be seen, by varying the wavelength used during the ablation process in the liquid, the size of the obtained particles increases, but their population density gradually decreases.

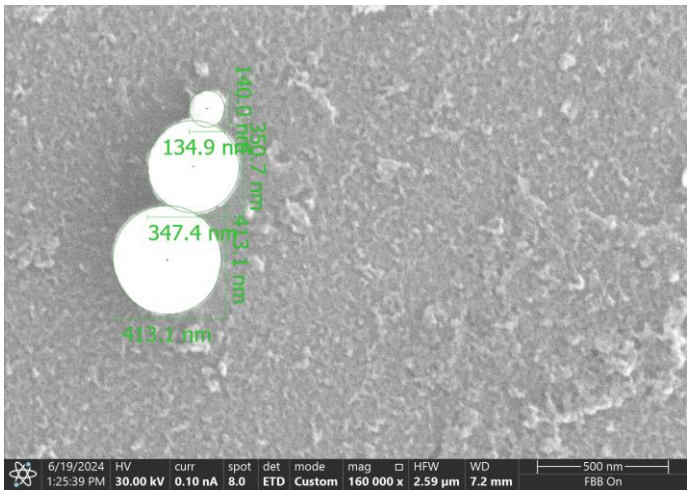


**Figure 12.** SEM characterization probe, 355nm, 400ml UPW

The image from below is a Transmission Electron Microscopy (TEM**)** image showing Ni nanoparticles, with colour overlays representing elemental mapping of different components, see figure 13. The nickel nanoparticles appear to be well-dispersed across the carbon grid.

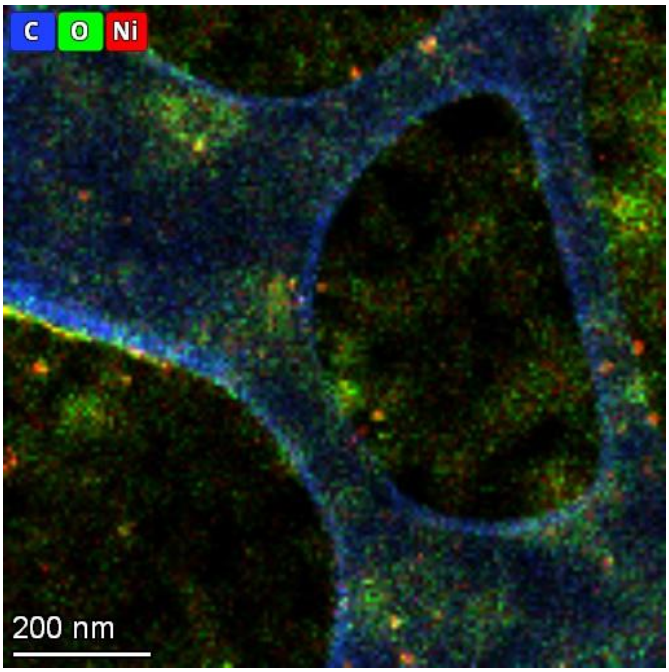


**Figure 13.** SEM characterization probe, 355nm, 400ml UPW

**Blue (C)**: Represents the presence of **carbon**, from a carbon grid used during the TEM analysis.

**Green (O)**: Represents oxygen, indicating possible oxidation of the nickel nanoparticles or the presence of an oxide layer on the surface.

**Red (Ni)**: Represents nickel, which corresponds to the actual nanoparticles observed in the image.

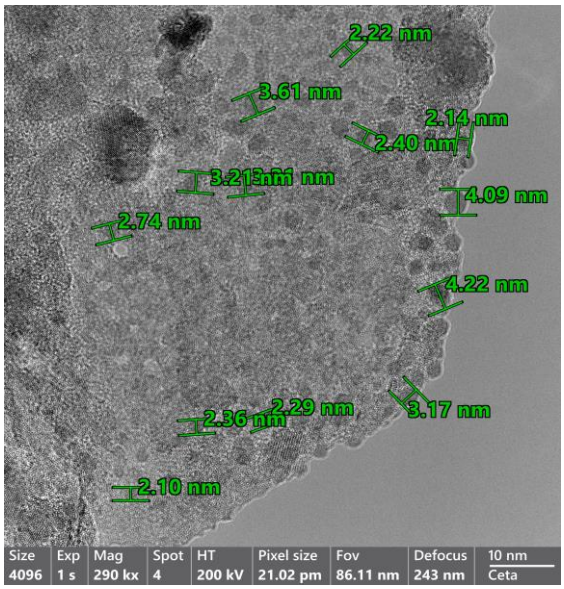


**Figure 14.** SEM characterization probe, 355nm, 400ml UPW

The green labels presented in image from above, figure 14 show measurements of nanoparticles at different regions ranging from approximately 2.10 nm to 4.22 nm.

## 4. CONCLUSION

DLS results here suggest that the synthesis process has yielded particles with a relatively consistent size. On average, the obtained samples have a polydispersity index of less than 0.7, indicating a narrow size distribution with cationic and anionic character.

EDX characterisation shows Nickel is distributed in small clusters or is relatively dispersed across the field of view. The concentration appears low overall, as indicated by the mostly dark colour, with brighter spots suggesting higher concentrations of Nickel in certain areas. One must consider the fact that no surfactant was added for preventing aggregation. From AFM images demonstrate uniform distribution of small nanoparticles on the analyzed probes.

TEM images provide a visual of Ni nanoparticles distributed on a carbon-based support, with some indication of oxidation (green oxygen mapping). The elemental mapping confirms the presence of these key components and suggests good dispersion of the particles at a nanoscale level.

## 5. ACKNOWLEDGEMENTS

It is stated that these applied contributions would not have been possible without the access to the available technical and material resources, to the equipment provided by the National Institute for the Physics of Lasers, Plasma and Radiation (INFLPR) and the expertise accumulated in this advanced field within the institute. Liquid laser ablation experiments were carried out at the Photonics and Plasma Innovation Center for Advanced Materials and Technologies (Photoplasmat C400).

## 6. REFERENCES

1. Overview on methods of synthesis of nanoparticles, Nilesh Patil1*, Rajveer Bhaskar, Vishal Vyavhare, Rahul Dhadge, Vaishnavi Khaire, Yogesh Patil, Int J Curr Pharm Res, Vol 13, Issue 2, 11-16, 2021.
2. Suryanarayana, C. (2001). Mechanical alloying and milling. *Progress in Materials Science, 46*(1–2), 1-184.
3. Mafuné, F., Kohno, J., Takeda, Y., Kondow, T., & Sawabe, H. (2000). Formation of gold nanoparticles by laser ablation in aqueous solution of surfactant. *Journal of Physical Chemistry B, 104*(39), 9111-9117.
4. Pfeiffer, K., Kley, E. B., & Chichkov, B. N. (1999). Fabrication of nanoparticle arrays by electron beam lithography. *Applied Surface Science, 139*(1–2), 12-16.
5. Chen, Y., & Zhang, L. (2010). Sub-10 nm patterning of nanoparticle arrays by focused ion beam. *Nano Research, 3*(12), 879-887.
6. Brinker, C. J., & Scherer, G. W. (2013). *Sol-gel science: The physics and chemistry of sol-gel processing*. Academic Press.
7. Bhushan, B. (2004). Chemical vapor deposition of coatings. In *Springer Handbook of Nanotechnology*. Springer, Berlin, Heidelberg.
8. Spanhel, L., & Anderson, M. A. (1991). Semiconductor clusters in the sol-gel process: quantized aggregation, gelation, and crystal growth in concentrated ZnO colloids. *Journal of the American Chemical Society, 113*(8).
9. Byrappa, K., & Yoshimura, M. (2012). *Handbook of Hydrothermal Technology*. William Andrew.
10. Capek, I. (2004). Preparation of metal nanoparticles in water-in-oil (w/o) microemulsions. *Advances in Colloid and Interface Science, 110*(1–2), 49-74.
11. Iravani, S. (2011). Green synthesis of metal nanoparticles using plants. *Green Chemistry, 13*(10), 2638-2650.
12. Lin, Y., Cui, X., (2005). Electrochemical deposition of metal nanoparticles on carbon nanotubes. *Nano Letters, 5*(9), 1939-1944.
13. Neel Narayan, Ashokkumar Meiyazhagan, Robert Vajtai, Metal Nanoparticles as Green Catalysts, Materials (Basel), November 2019
14. Isao Matsui, Nanoparticles for Electronic Device Applications: A Brief Review, Journal of Chemical Engineering of Japan, Vol 38, No 8, 2005, 536-546.